Earth and Planetary Science Letters 288 (2009) 228–234

Contents lists available at ScienceDirect

Earth and Planetary Science Letters

journal homepage: www.elsevier.com/locate/epsl

Experimentally determined Si isotope fractionation between silicate and Fe metal and implications for Earth's core formation

Anat Shahar [a,b,*], Karen Ziegler [c], Edward D. Young [a,c], Angele Ricolleau [b], Edwin A. Schauble [a], Yingwei Fei [b]

[a] Department of Earth and Space Sciences, University of California Los Angeles, 595 Charles Young Drive East, Los Angeles, CA 90095, USA
[b] Geophysical Laboratory, Carnegie Institution of Washington, 5251 Broad Branch Rd. NW, Washington DC 20015, USA
[c] Institute of Geophysics and Planetary Physics, University of California, Los Angeles, 3845 Slichter Hall, Los Angeles, CA 90095, USA

ARTICLE INFO

Article history:
Received 20 April 2009
Received in revised form 14 August 2009
Accepted 12 September 2009
Available online 12 October 2009

Editor: L. Stixrude

Keywords:
core formation
silicon isotope
metal–silicate partitioning
high pressure
high-temperature

ABSTRACT

Stable isotope fractionation amongst phases comprising terrestrial planets and asteroids can be used to elucidate planet-forming processes. To date, the composition of the Earth's core remains largely unknown though cosmochemical and geophysical evidence indicates that elements lighter than iron and nickel must reside there. Silicon is often cited as a light element that could explain the seismic properties of the core. The amount of silicon in the core, if any, can be deduced from the difference in $^{30}Si/^{28}Si$ between meteorites and terrestrial rocks if the Si isotope fractionation between silicate and Fe-rich metal is known. Recent studies (e.g., [Georg R.B., Halliday A.N., Schauble E.A., Reynolds B.C., 2007. Silicon in the Earth's core. Nature 447 (31), 1102–1106.]; [Fitoussi, C., Bourdon, B., Kleine, T., Oberli, F., Reynolds, B. C., 2009. Si isotope systematics of meteorites and terrestrial peridotites: implications for Mg/Si fractionation in the solar nebula and for Si in the Earth's core. Earth Planet. Sci. Lett. 287, 77–85.]) showing (sometimes subtle) differences between $^{30}Si/^{28}Si$ in meteorites and terrestrial rocks suggest that Si missing from terrestrial rocks might be in the core. However, any conclusion based on Earth–meteorite comparisons depends on the veracity of the $^{30}Si/^{28}Si$ fractionation factor between silicates and metals at appropriate conditions. Here we present the first direct experimental evidence that silicon isotopes are not distributed uniformly between iron metal and rock when equilibrated at high temperatures. High-precision measurements of the silicon isotope ratios in iron–silicon alloy and silicate equilibrated at 1 GPa and 1800 °C show that Si in silicate has higher $^{30}Si/^{28}Si$ than Si in metal, by at least 2.0‰. These findings provide an experimental foundation for using isotope ratios of silicon as indicators of terrestrial planet formation processes. They imply that if Si isotope equilibrium existed during segregation of Earth's core-forming metal and silicate mantle, there should be an isotopic signature of Si in the core. Our experiments, combined with previous measurements of Si isotope ratios in meteorites and rocks representing the bulk silicate Earth, suggest that the formation of the Earth's core imparted a high $^{30}Si/^{28}Si$ signature to the bulk silicate Earth due to dissolution of ~6 wt% Si into the early core.

1. Introduction

As early as 1952, Francis Birch noted that seismic velocities were inconsistent with an outer core of pure iron and nickel; the core exhibits a density deficit of about 5 to 10% (Birch, 1952). In that paper, and the one succeeding it (Birch, 1964), Birch suggested that the low density was due to the presence of one or more light elements dissolved in Fe–Ni alloy. Candidate elements include carbon, hydrogen, sulfur, silicon, and oxygen. Since then many studies have sought to determine which of these elements are responsible for lowering the density of the core (see Li and Fei, 2004, for a review).

Chondritic meteorites (the most primitive rocks of the solar system) are thought to be a first-order proxy for the bulk composition of Earth because the relative abundances of refractory major elements comprising these rocks are indistinguishable from those of the Sun. Chondritic ratios of rock-forming elements are also found for dust surrounding other stars (Zuckerman et al., 2007). On close examination, however, one finds that the bulk silicate Earth (BSE) has a greater Mg/Si than chondrites by ~15% (Ringwood, 1989). Since volatility was a primary mechanism for fractionating elements in the early solar system, and silicon and magnesium have similar volatilities, this discrepancy is unexpected. There are several possible explanations for the super-chondritic Mg/Si, including non-chondritic starting materials, or sequestration of Si into the core. A deficit in Si in bulk silicate Earth (as opposed to Mg-excess) is supported by super-chondritic Al/Si of Earth relative to chondrites (Palme and O'Neil, 2003).

Geochemical arguments for the light element composition of the core based on calculations of mass balance assuming a chondritic

* Corresponding author. Geophysical Laboratory, Carnegie Institution of Washington, 5251 Broad Branch Rd. NW, Washington DC 20015, USA. Tel.: +1 202 478 8910.
E-mail address: ashahar@ciw.edu (A. Shahar).

0012-821X/$ – see front matter © 2009 Elsevier B.V. All rights reserved.
doi:10.1016/j.epsl.2009.09.025

Earth are presently poorly constrained. Estimates for the concentration of Si in the core range up to 14 wt% (e.g., O'Neil, 1991; Wänke and Dreibus, 1997). Experiments have shown that silicon is a plausible light element in the core because liquid iron reacts with silicate to form a silicon–iron alloy at relevant pressures and temperatures (e.g., Knittle and Jeanloz, 1989; Lin et al., 2002; Dubrovinsky et al., 2003). Equilibration of $MgSiO_3$ with pure iron at high pressure and temperature (26 GPa, 2500 °C) results in more than 2% silicon in the metal phase (Ito et al., 1995). Recent compressional sound velocity measurements of iron alloys at high pressure showed that the incorporation of small amounts of silicon (~5%) or oxygen are compatible with geophysical observations (Badro et al., 2007). Therefore, while it has been shown that silicon does alloy with iron under reducing conditions, at high pressure and temperature, and these alloys are consistent with the geophysical constraints, it is still unclear whether this reaction actually occurred in the Earth and to what extent.

In the absence of direct samples from the core, Georg et al. (2007) sought to test the idea that there is substantial Si in the core by comparing the Si isotopic composition of Earth's mantle to chondrites. They found that the Earth has 0.2‰ (parts per thousand) higher $^{30}Si/^{28}Si$ than chondrites and concluded that the difference is a consequence of $^{30}Si/^{28}Si$ fractionation between the core and mantle. Since then, several studies have measured the silicon isotope ratios between Earth and chondrite and have found variable results (e.g., Fitoussi et al., 2009; Armytage et al., 2009). Theoretical estimates of the metal–silicate $^{30}Si/^{28}Si$ partitioning at low pressure are consistent with the Georg et al. (2007) conclusion, but until now there has been no experimental evidence at any pressure or temperature to determine if there is indeed a substantial $^{30}Si/^{28}Si$ fractionation between metal and silicate, the basis for the original argument of Georg et al. (2007). High pressure is likely to stiffen bonds in typical materials (the precise relationship being a function of mode Grüneisen parameters), potentially changing inter-phase fractionation factors (Polyakov and Kharlashina, 1994). Given the uncertainties inherent in theoretical calculations, experiments are necessary for validating the use of Si isotope ratios as indicators of Si in the core.

There have been no silicon isotope experiments conducted at high pressure and temperature in part because of difficulties in high-precision Si isotope ratio measurements on small samples and in extracting silicon from experimental products. Recent iron isotope experiments (Poitrasson et al., 2009) at high pressure and temperature (2000 °C, 7.7 GPa) have found no iron isotope fractionation between metal and silicate. However, enhancement of isotope fractionation by pressure is potentially important at pressures higher than 7.7 GPa (Polyakov, 2009). Therefore, more experiments are needed at higher pressure to validate predictions and explore the potential for iron isotopic fractionation during core formation.

In this study we conducted experiments to measure the Si isotopic fractionation between Fe liquid metal (core analog) and silicate melt (the mantle) at conditions relevant to core formation (although not coincident with core formation), using ^{28}Si-spiked starting material and a newly-developed silicon extraction technique. The results provide an independent constraint on the amount of silicon in the Earth's core, if any.

2. Methodology

2.1. High pressure experiments

Experiments were performed at the Carnegie Institution of Washington's Geophysical Laboratory on a ½-in. piston cylinder apparatus. The cell assembly consists of a graphite tube heater insulated by a pyrex glass sleeve and talc shell. The W/Re thermocouple is inserted into the sample chamber through a small hole in the stainless steel base plug, which is surrounded by a small pyrophyllite sleeve. Graphite capsules were used in all of the experiments. Experiments were conducted at 1 GPa and 1800 °C for durations ranging from 1 to 30 min. The starting material consisted of a silicate-oxide mix of Al_2O_3, MgO, SiO_2, CaO, and Fe_2O_3 in proportions approximately representing a pyrolitic BSE composition, and a metallic iron–silicon alloy powder ($Fe_{91}Si_9$, Goodfellow) representing the core. Starting with 9 at.% Si in the metal reduces the oxygen fugacity of the experimental charge so that some Si is retained in the metal. The silicate starting material was spiked with ^{28}Si in order to trace the exchange of Si between silicate and metal (see below).

Major and minor element contents of the experimental charges were measured using the 5-spectrometer JEOL 8900 electon probe microanalyzer (EPMA) at the Geophysical Laboratory. We used a series of silicate, oxide, and metal standards and conditions of 30 nA beam current and 15 kV accelerating voltage. Analyses were reduced using a ZAF correction routine. After analysis with the EPMA, the samples were crushed and handpicked. Silicate and metallic portions were easily separated under a bifocal microscope and only portions that were >99% of a single phase were dissolved for isotopic analysis.

2.2. Sample dissolution and chemistry

Silicate samples and standards (NBS-28; IRMM-018a, Diatomite, BigBatch, Reynolds et al., 2007; San Carlos olivine) were dissolved in 2.5 M HF at ~120 °C in sealed Savillex™ beakers. The volume of 2.5 M HF used is dictated by the Si-concentration of the silicate, and by a final target concentration of fluosilicate ions below 40 mM, in order to avoid volatilization of SiF_4 (De La Rocha et al., 1996). Concentrated HNO_3 was added to accelerate dissolution, if required, without adding additional F^--ions. Samples of dissolved Si in 2.5 M HF were diluted by a factor of 250 to produce a 4.6 ppm Si solution containing 0.02% HF, suitable for further processing. The solutions ready for ion exchange column chemistry have a pH of 2.0.

Metals were dissolved in concentrated HCl to yield Fe in solution and a silica gel according to the simplified reactions:

$$FeSi_s + 6HCl_{aq} \rightarrow FeCl_{2_{aq}} + SiCl_{4_{aq}} + 3H_2$$

$$SiCl_{4_{aq}} + 2H_2O \rightarrow SiO_{2_{gel}} + 4HCl_{aq},$$

where the second reaction is so rapid as to preclude loss of Si as the volatile $SiCl_4$ (Bauer & Deiss, 1915). The dissolved metal solution is dried down at 100 °C, and the silica is dissolved in 2.5 M HF as described above. These solutions have a pH of 2.0 to 2.2 prior to ion exchange chromatography.

Separation of Si from other ions was achieved by ion exchange chromatography following the method described by Georg et al. (2006). The method relies on the fact that cation exchange resins do not retain major aqueous Si species. The exchange columns contain 2.0 ml of Bio-Rad™ AG 50 W-X12 cation exchange resin in 200 to 400 mesh hydrogen form. The resin is pre-cleaned by repeated rinsing with HCl, HNO_3 and MQ-e water (pH neutral, 18.5 MΩ). Column loads consist of 3.6 μg of sample Si in 0.02% HF. Silicon is then eluted with 6 ml of MQ-e water. The resulting solution has a final Si-concentration of ~0.5 ppm, and an HF-concentration of 0.002%. Fig. 1 shows an elution curve for silicon following this procedure. Similar elution curves were obtained for silicon loadings of up to 11 μg. Following the elution of Si, the retained cations are stripped from the resin with several HCl and HNO_3 rinses (see Georg et al., 2006 for details), and the resin is returned to pH-neutrality with MQ-e H_2O rinsing. All acids used in the sample dissolution and Si separation steps are ultra-pure double-distilled acids.

The international reference Si isotope standard is NBS-28, which has, per definition, a $\delta^{30}Si$ value of 0.0‰. We used NBS-28 as a primary standard in this study. The standard was dissolved and purified in the same manner as described above for the samples. We also used an in-

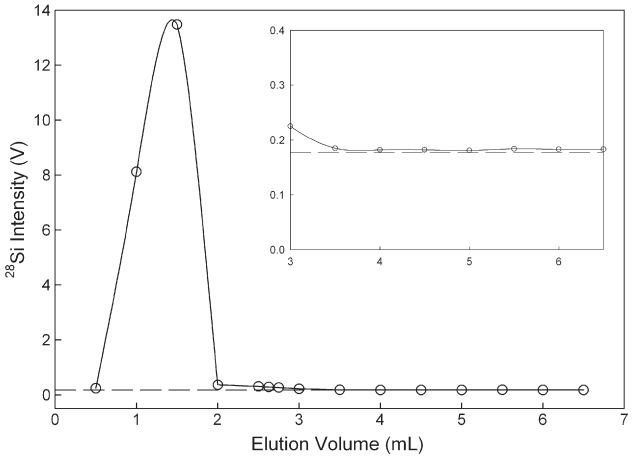

Fig. 1. Typical elution curve for Si. 3.6 μg of Si were loaded onto the column in 0.02% HF and then eluted with MQ-e water.

house secondary standard of tetraethyl orthosilicate, hydrolyzed under stirring in MQ-e water to produce pure Si solution (TEOS). The TEOS standard has a $\delta^{30}Si_{NBS\text{-}28}$ value of −2.15‰ +/−0.02 (2se) based on multiple determinations.

In order to verify the accuracy of the analytical techniques, we conducted various tests. Firstly, we tested the exchange column procedure by processing aliquots of the pure TEOS solution through the entire column chemistry, and comparing the isotopic composition of the eluted Si to the known value for this standard. No Si isotopic fractionation was seen.

Secondly, we tested the potential for matrix effects on the effectiveness of the Si separation of the exchange columns. We prepared a solution representing a typical forsterite-rich silicate by mixing Spex CertiPrep™ element solutions with the TEOS solution (7.41 μg Al, 90.14 μg Si, 83.09 μg Mg, 0.29 μg Fe, 7.72 μg Ca in 1 ml MQ-e water), and passed it through the exchange columns using our standard procedures. The eluted Si-bearing solutions were inspected for traces of the matrix elements, and analyzed for $^{29}Si/^{28}Si$ and $^{30}Si/^{28}Si$. No measurable amounts of the other elements were found to be eluted with Si. The Si isotopic composition was not affected by the presence of these other elements in the chemistry procedure (Table 1).

Thirdly, we tested the ability of the exchange columns to remove large amounts of Fe from the metal solutions without affecting the recovery and isotopic composition of the relatively small amounts of Si. A $Fe_{91}Si_9$-solution was prepared by mixing Spex CertiPrep Fe-solution with dissolved NBS-28, and processed through the exchange columns. Eluting Si was collected in 0.5 ml aliquots and inspected for trace amounts of Fe. None of the aliquots contained measurable concentrations of Fe. The various acids used subsequently to remove the Fe from the exchange resin were collected and inspected for traces of Si that might have been retained on the resin with the Fe; no significant amounts of Si were detected.

Fourthly, we tested the validity of dissolving Si in concentrated HCl without isotopic fractionation due to loss of Si as $SiCl_4$ by mixing an aliquot of pure TEOS solution with concentrated HCl, evaporating at 50 °C and 140 °C, and dissolving the precipitated Si-gel according to the HF-procedure described above for silicates. No significant isotopic fractionation of the Si was observed (Table 2).

Lastly, we tested our entire analytical protocol (sample dissolution, cation exchange chemistry, and mass spectrometry) by measuring available international Si isotope standards. We analyzed three Si isotope samples regarded as standard materials (IRMM-018a, Diatomite, Big Batch) that were previously measured in an inter-laboratory comparison by 8 different laboratories (Reynolds et al., 2007). Our

Table 1
Silicon isotope ratios for solutions of Al, Si, Ca, and Mg: 7.41 μg Al, 90.14 μg Si, 83.09 μg Mg, 0.29 μg Fe, 7.72 μg Ca.

Column-run no.	$\delta^{29}Si$	St. err.	$\delta^{30}Si$	St. err.	$\Delta^{29}Si$	St. err.	*n*
Experiment 2							
2-1	−0.097	0.032	−0.222	0.030	0.018	0.030	5
2-2	−0.156	0.041	−0.196	0.031	−0.055	0.045	5
2-3	−0.007	0.025	0.037	0.027	−0.027	0.032	8
2-4	0.073	0.012	0.064	0.020	0.039	0.016	8
2-5	−0.049	0.019	−0.089	0.018	−0.003	0.024	8
2-6	−0.077	0.016	−0.179	0.021	0.016	0.020	8
2-7	0.059	0.007	0.085	0.018	0.015	0.008	16
Avg.	−0.036		−0.071		0.001		7
St.dev.	0.083		0.132		0.032		
St.err.	0.031		0.050		0.012		
Experiment 3							
3-1	−0.171	0.031	−0.183	0.026	−0.076	0.040	5
3-2	0.111	0.018	0.330	0.026	−0.060	0.014	5
3-3	−0.027	0.022	0.028	0.017	−0.042	0.027	8
3-4	0.068	0.012	0.011	0.020	0.062	0.017	8
3-5	−0.029	0.012	0.027	0.026	−0.043	0.016	8
3-6	−0.051	0.018	0.052	0.012	−0.078	0.022	8
3-7	0.051	0.009	0.117	0.013	−0.010	0.008	16
Avg.	−0.007		0.054		−0.035		7
St.dev.	0.094		0.153		0.049		
St.err.	0.035		0.058		0.018		
Experiment 4							
4-1	0.106	0.014	0.314	0.031	−0.056	0.012	5
4-2	−0.020	0.016	0.051	0.026	−0.047	0.013	8
4-3	−0.079	0.023	−0.098	0.014	−0.028	0.023	8
4-4	−0.048	0.014	−0.063	0.011	−0.015	0.017	8
4-5	−0.074	0.015	0.049	0.022	−0.099	0.009	8
4-6	0.028	0.009	0.085	0.013	−0.016	0.011	16
Avg.	−0.014		0.056		−0.044		6
St.dev.	0.071		0.145		0.032		
St.err.	0.029		0.059		0.013		
Experiment 5							
5-1	0.083	0.023	0.371	0.014	−0.109	0.020	5
5-2	−0.044	0.018	−0.018	0.019	−0.035	0.024	8
5-3	−0.042	0.017	−0.001	0.020	−0.041	0.013	8
5-4	−0.293	0.012	−0.347	0.011	−0.113	0.013	8
5-5	−0.051	0.018	−0.080	0.026	−0.009	0.015	8
5-6	−0.004	0.053	−0.101	0.059	0.048	0.078	16
Avg.	−0.058		−0.029		−0.043		6
St.dev.	0.125		0.232		0.061		
St.err.	0.051		0.095		0.025		
All experiments							
Avg.	−0.028		0.002		−0.029		26
St.dev.	0.091		0.167		0.046		
St.err.	0.018		0.033		0.009		

Each datum is a separate run through the indicated column and is the mean of ~5 blocks by MC-ICPMS.

$\delta^{30}Si$ results are within <0.1‰ of the average values obtained by Reynolds et al. (2007) (Table 3). In addition, we analyzed a separate of San Carlos olivine (mantle xenolith olivine). This is not a recognized standard but it is representative of a material with a more complicated matrix chemistry that other laboratories have analyzed over the years. We obtain a $\delta^{30}Si$ relative to NBS-28 of −0.28 +/−0.03 (2se)

Table 2
Isotopic measurements of TEOS Si relative to the TEOS standard values following mixing with concentrated HCl, evaporation at the specified temperature, and dissolution of the precipitated Si-gel according to the HF-procedure described in the text.

	$\delta^{29}Si$	2se	$\delta^{30}Si$	2se
TEOS in HCl, 50 °C	0.055	0.050	0.097	0.016
TEOS in HCl, 140 °C	0.012	0.048	0.071	0.051

Table 3
Measured Si isotope ratios for Si isotope standards analyzed as part of this study compared with values from the literature.

Standard		δ^{29}Si	2se	δ^{30}Si	2se	n
IRMM-018a	UCLA	−0.791	0.012	−1.549	0.092	2
	Reynolds et al. (2007)	−0.850	0.01	−1.650	0.01	
Diatomite	UCLA	0.630	0.004	1.215	0.089	1
	Reynolds et al. (2007)	0.640	0.02	1.260	0.02	
Big Batch	UCLA	−5.332	0.126	−10.384	0.296	2
	Reynolds et al. (2007)	−5.350	0.02	−10.480	0.04	
Mantle olivine	UCLA, SC olivine[a]	−0.147	0.014	−0.281	0.032	5
	Georg et al. (2007)[b]	−0.15	0.03	−0.33	0.03	20
	Douthitt (1982)[c]	n/a		−0.3	0.1	1

[a] SC = San Carlos.
[b] Average of 2 olivines from Cameroon line spinel lherzolite.
[c] Olivine from a dunite from N.C.

compared with values from other mantle olivine samples of −0.33 +/−0.03 and −0.3 +/− 0.1 by Georg et al. (2007) and Douthitt (1982, and references therein), respectively.

2.3. Isotope ratio analyses

In preparation for isotopic analyses, the solutions derived from exchange columns (Si in 0.002% HF) were spiked with concentrated HNO_3 to obtain a 2% HNO_3 solution. Special attention was paid to precise matching of the acid matrix of the standard solutions (2% HNO_3, 0.002% HF).

Silicon isotope mass spectrometry of purified solutions of Si was performed on the UCLA ThermoFinnigan Neptune MC-ICPMS. Samples were run in dry plasma mode by using the Cetac Aridus™ I desolvating system, the Cetac PFA microconcentric Aspire™ nebulizer with a 50 µl/min uptake rate, and a PFA spray chamber. We measure $^{28}Si^+$, $^{29}Si^+$, and $^{30}Si^+$ intensities simultaneously. Each Faraday cup collector is linked to amplifiers with 10^{11} Ω resistors. Ion beam intensities for the ~0.5 ppm analyte solutions and standard solutions were between 150 and 200 mV on $^{29}Si^+$, with backgrounds of <5 mV. The presence of 0.002% HF in the solution and the use of a glass torch body did not add measurably to the normal Si background signal. The MC-ICPMS was operated at a mass resolving power (instrumental $m/\Delta m$) of ~12,000 (corresponding to a flat-top peak mass resolution of ~4000). The high mass resolution eliminates potential molecular interferences from $^{28}N_2^+$ and $^{12}C^{16}O^+$ for $m/z=28$, $^{14}N^{15}N^+$ and $^{12}C^{17}O^+$ for $m/z=29$, and $^{14}N^{16}O^+$ and $^{12}C^{18}O^+$ for $m/z=30$. Potential doubly charged mass interference species and their first ionization potentials include $^{56}Fe^{2+}$ (m/z~28, 16.18 eV), $^{58}Ni^{2+}$ (m/z~29, 18.15 eV), $^{58}Fe^{2+}$ (m/z~29, 16.18 eV), and $^{60}Ni^{2+}$ (m/z~30, 18.15 eV). All of these doubly ionized species have first ionization potentials substantially greater than that of Ar^+ (15.76 eV), with the result that none appears as a detectable species in the mass spectrum under our operating conditions. Nonetheless, we checked for these possible interferences and found no evidence for their presence. In all cases corrections for instrumental mass bias (~5%) were performed by sample-standard bracketing with peak height matching between sample and standard to better than 5%. Instrumental drift is typically no more than 0.5‰ over the course of several hours, which is much slower than the rate of sample data collection. Solutions are generally measured in blocks of 20 cycles with ~4 s integrations per cycle. A typical analysis comprised 10 blocks of 20 cycles. Internal precision for the measurements reported here is better than +/− 0.1‰ (2σ) per amu and usually near 0.04‰ based on replicate analyses of standards. The external reproducibility of our in-house silicon standard taken through the column chemistry with a typical silicate matrix, shown in Table 2, is similar to the internal precision reported here for each experimental product.

2.4. Equilibrium

In order to establish equilibrium fractionation factors we used the three-isotope exchange method first described by Matsuhisa et al. (1978) and adapted to mineral–mineral fractionation factors by Shahar et al. (2008). In the present context of three Si isotopes a condition for equilibrium among the Si isotopes between two phases i and j is $\alpha_{i-j}^{29/28}=(\alpha_{i-j}^{30/28})^{\gamma}$ where $\alpha_{i-j}^{29/28}={}^{29}R_i/{}^{29}R_j$, ${}^{29(30)}R_i=({}^{29(30)}Si/{}^{28}Si)_i$ for phase i, and the exponent γ relating the three isotopes at equilibrium is

$$\gamma=\frac{\frac{1}{m_{29}}-\frac{1}{m_{28}}}{\frac{1}{m_{30}}-\frac{1}{m_{28}}} \quad (1)$$

where m is the mass of subscripted Si isotope. In this case $\gamma=0.5178$. Isotopic compositions representing equilibrium lie on a curve that is closely approximated by a line on a plot of δ^{29}Si vs. δ^{30}Si ($\delta^{29,30}$Si is the per mil deviation in $^{29,30}Si/^{28}Si$ from a reference) with a slope of γ. This is a necessary criterion for equilibrium. The principle of the three-isotope exchange method in this context is to replace the silicon terrestrial fractionation line (TFL) on plots of δ^{29}Si vs. δ^{30}Si, representing normal terrestrial silicon, with a secondary fractionation line (SFL) that represents the condition for equilibrium in the experiments. The two lines share the same slope γ but have distinct intercepts reflecting their different amounts of ^{28}Si due to the ^{28}Si spike present in the experiments (Fig. 2). The equation

$$\delta^{29}Si_i=\gamma\delta^{30}Si_i+(\delta^{29}Si_0-\gamma\delta^{30}Si_0) \quad (2)$$

relates the equilibrium Si isotope ratios for phase i on the SFL where $\delta^{29}Si_0$ and $\delta^{30}Si_0$ are the δ values for the total Si comprising the spiked experimental system. The last term in the equation is the intercept on the Si three-isotope plot.

3. Results

3.1. Run product characterization

Typical EPMA analyses of the experimental run products are shown in Table 4. These analyses were obtained after polishing the samples and before crushing them for isotopic analysis. There is 8 wt% silicon in all three metal products and 0.1% FeO in the silicate melt, imparting an oxygen fugacity ~4 log units below the Fe (Iron)–FeO

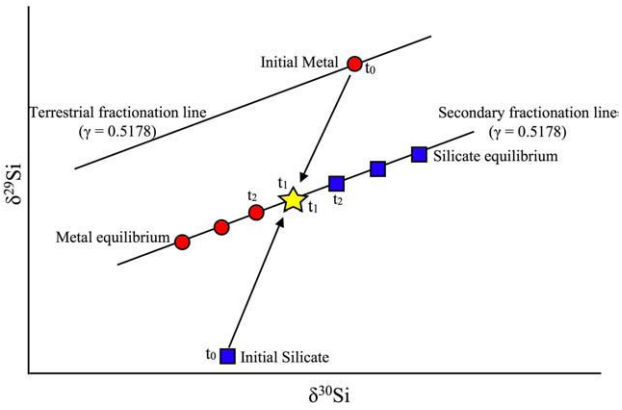

Fig. 2. A schematic of the three-isotope exchange method used in this study where all the constituents in the capsule mix together at first and then move towards equilibrium along a secondary fractionation line. The metal (circles) starts on the terrestrial fractionation line while the silicate (squares) begins off the terrestrial fractionation line due to addition of ^{28}Si. Silicon in both phases migrates towards a secondary fractionation line (SFL) representing a condition for isotopic equilibrium. With time equilibrium Si isotope ratios are established along the SFL. The star represents the bulk Si isotopic composition of the system.

Table 4
Typical EMPA analyses of the metallic and silicate phases.

Metal	Mass%	Oxide	Mass%
Al	0.00	Al_2O_3	3.94
Si	8.05	SiO_2	54.08
Mg	0.00	MgO	38.65
Fe	91.67	FeO	0.10
Ca	0.00	CaO	3.02
Total	99.72	Total	99.79

(Wüstite) buffer (~IW-4) in all experiments. The phases were homogeneous in their Si concentrations, suggesting equilibration of Si. As shown in Shahar et al. (2008), attainment of chemical equilibrium in piston cylinder experiments can be faster than isotopic equilibration. At the conditions of these experiments we expect chemical equilibrium to be attained on the order of tens of seconds (Thibault and Walter, 1995).

3.2. Isotopic results

Isotopic results are shown in Table 5. While Si in the metal portion of the experimental charge began on the terrestrial fractionation line, in all experiments it has moved off of that line in three-isotope space so that the metal product becomes more depleted in $^{30(29)}Si/^{28}Si$ than the silicate (Fig. 3). This demonstrates the high degree of Si mobility in the charge; by tracing the isotopes in these experiments we are able to quantify the movement of Si originating from the initial silicate phase into the metal phase and vice-versa.

The data for 1-minute experimental runs yield Si in metal and in silicate melt with nearly identical $\delta^{30}Si$ and $\delta^{29}Si$ values, indicating thorough mixing prior to isotopic equilibration (Fig. 3). Longer runs of 10 and 30 min show the isotopes separating towards their equilibrium ratios along secondary fractionation lines. We note that although the silicate began with significantly lower $^{30}Si/^{28}Si$ and $^{29}Si/^{28}Si$ (10 ‰) than the metal due to the addition of ^{28}Si, the end products show the silicate melt more enriched in the heavy isotopes than the metal, giving us confidence that the metal and silicate melt readily exchanged isotopes.

4. Discussion

4.1. Equilibrium and oxygen fugacity

Fig. 2 depicts the behavior of experiments in three-isotope space for a sample that mixes thoroughly and then equilibrates. Mixing followed by unmixing is relevant for this study because the samples begin grossly out of chemical equilibrium with regard to the concentration of silicon between metal and silicate. In this situation the silicon isotope ratios for both phases (metal and silicate) become equal due to thorough mixing as Si diffuses in and out of the metal and silicate in response to the Si chemical potential gradients imposed by

Table 5
Experimental results.

Name	Phase	Temp (°C)	Pressure (GPa)	Time (min)	$\delta^{29}Si$ (‰)	1σ	$\delta^{30}Si$ (‰)	1σ	$\Delta^{29}Si$[a] (‰)
Start	Silicate	–	–	–	−10.54	0.005	−10.39	0.01	−5.16
Start	Metal	–	–	–	0.32	0.027	0.54	0.05	0.05
PC637	Silicate	1800	1	30	−4.28	0.020	−3.79	0.04	−2.32
PC637	Metal	1800	1	30	−5.58	0.032	−5.66	0.06	−2.65
PC639	Silicate	1800	1	10	−4.38	0.015	−4.05	0.02	−2.28
PC639	Metal	1800	1	10	−5.50	0.016	−5.48	0.03	−2.66
PC638	Silicate	1800	1	1	−4.76	0.030	−4.48	0.04	−2.45
PC638	Metal	1800	1	1	−4.94	0.030	−4.53	0.04	−2.54

[a] $\Delta^{29}Si = \delta^{29}Si - (\delta^{30}Si * 0.5178)$.

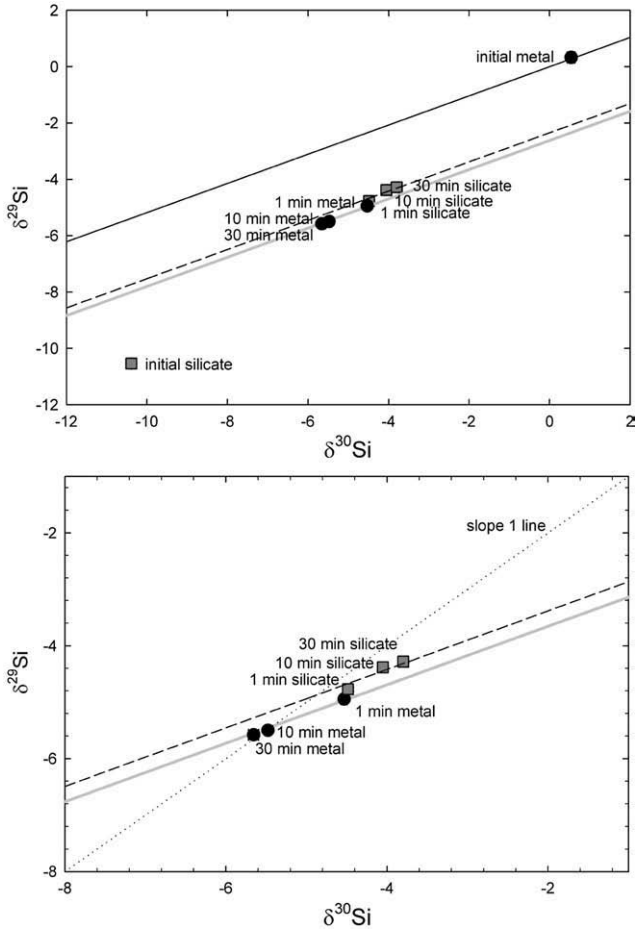

Fig. 3. Silicon three-isotope plot showing the experimental determination of Si isotopic fractionation between silicate and Fe metal at 1 GPa and 1800 °C. Upper plot shows all data points while the lower plot is a close-up showing the data near equilibrium. The close-up shows the separation of metal and silicate melt Si isotope ratios along a mass fractionation trajectory and deceleration of isotope shifts with time, indicating an approach to equilibrium. Symbols: solid — SFL, dashed — line with same slope as SFL going through silicate melt values. Errors are 1se.

the fO_2 of the experimental charge. Following mixing to attain chemical equilibrium there is an "unmixing" among the isotopes of Si along the secondary fractionation line as the system equilibrates isotopically as well as chemically.

The experiments were performed in a graphite capsule so as to keep the oxygen fugacity low in the experiments and so to retain as much Si in the metal as possible. Under the conditions of these experiments (and presumably during core formation) silicate melts are expected to contain Si^{4+} bound almost exclusively to oxygen while the metal contains metallic Si, dominantly bonding with iron. High-temperature equilibrium isotopic fractionation is mainly determined by the sum of bond force constants acting on the atom of interest (e.g., Bigeleisen and Mayer, 1947). Therefore, the isotope fractionation between the metal and silicate melts depends on the differences in the force constants associated with Si–O and Si–Fe bonds. It is not dependent upon the concentration of the silicon in the metal because there is no relationship between the abundance of Si and the strength and stiffness of the Si–Fe bonds (as long as Fe>>Si). Therefore, the oxygen fugacity in our experiment is only an important parameter in so far as it must be kept low to ensure that there is enough Si in the metal for reliable isotopic analysis; oxygen fugacity does not affect isotope fractionation factors. However, by choosing to use graphite capsules, our experimental charges become open to Si by virtue of loss of Si to graphite. The amount of Si lost is different in each of our experiments (see below).

The deceleration in the rate of Si isotope exchange after 10 min in these experiments (Fig. 3) suggests that the 30 min runs represent a close approach to isotopic equilibrium with Si in silicate melt 2.0‰ greater in $^{30}Si/^{28}Si$ than Si in the metal. The silicon isotopic ratios of the silicate melt and metal phases are on similar, but not identical, secondary fractionation lines separated by about 0.2‰. By 30 min the fractionation is 10 times larger than the discrepancy between the two SFLs, implying that the departure from equilibrium is relatively small. The deviations from a single fractionation line are most likely due to the silicon loss to the carbon capsule. Fig. 4 shows the isotope ratio data compared with the bulk value of each experiment and the calculated bulk value, assuming a closed system in the latter case. Each experiment has a different bulk Si isotopic composition causing the scatter from the calculated experimental secondary fractionation line. In order to determine the amount of Si lost, the fractionation factor must be known between the silicon lost to the graphite and that which remained in the experimental charge. This factor is not known, but one could postulate that the fractionation between silicate and metal is similar to that between silicate and graphite as the silicon lost to the capsule and that which goes into the metal are both reduced. Therefore, using the fractionation factor determined in this study as an estimate for the fractionation between the silicate melt and graphite capsule, one calculates loss of 7% of total Si to the capsule in the 1-minute experiment, 9% in the 10-minute experiment and 10% in the 30-minute experiment. However, we emphasize that such losses of Si to the capsule, and the precise location of the final SFL are irrelevant if a close approach to equilibrium is attained, as in these experiments.

4.2. Si in the core

Our results show that there is at least a 2‰ $^{30}Si/^{28}Si$ fractionation between Si in silicate and Si in metal at high pressure and temperature, i.e., $\Delta^{30}Si_{silicate-metal} = \delta^{30}Si_{silicate} - \delta^{30}Si_{metal} > 2.0‰$. Using the experimentally determined fractionation factor for $^{30}Si/^{28}Si$ between silicate and metal, we can estimate the amount of silicon in the core from mass balance:

$$\Delta^{30}Si_{BSE}X_{Si} + \delta^{30}Si_{Core}(1 - X_{Si}) = \delta^{30}Si_{chondrite}. \quad (3)$$

Here $\delta^{30}Si_{BSE}$ is the $^{30}Si/^{28}Si$ value of the bulk silicate Earth, X_{Si} is the fraction of the Earth's silicon that is in the silicate portion of the planet, $\delta^{30}Si_{Core}$ is the $^{30}Si/^{28}Si$ value of the core and $\delta^{30}Si_{chondrite}$ is the $^{30}Si/^{28}Si$ value of chondrites (where we assume $\delta^{30}Si_{chondrite}$ represents $\delta^{30}Si$ for the bulk Earth, core and mantle together). For this calculation we use BSE $\delta^{30}Si = -0.38‰$ and chondrite $\delta^{30}Si = -0.58‰$ (Georg et al., 2007). Formation of the Earth's core almost certainly occurred at pressures and temperatures beyond those sampled by our calibration experiments. We use theoretical metal–silicate fractionation models to try to constrain pressure and temperature effects and then use our experimental value to anchor the calculations. The results enable extrapolation to the pressures and temperatures appropriate for core formation (e.g. 25 GPa, 2500 K).

Temperature is a critical parameter for isotope fractionation and typical equilibrium fractionations scale with T^{-2} for temperatures greater than ~1000 K (Bigeleisen and Mayer, 1947). Pressure effects, generally considered secondary or negligible in stable isotope geochemistry, could become important because of fundamental changes in the silicate melt structure at depth in Earth. Molecular dynamics studies (e.g., Stixrude and Karki, 2005) suggest that Si undergoes a continuous transition from 4-fold (tetrahedral, Si^{IV}) coordination in low pressure melts to 6-fold (octahedral, Si^{VI}) coordination at 135 GPa, the latter pressure corresponding to the modern core–mantle boundary. In order to assess the effects of pressure we calculated equilibrium fractionations between iron silicide (Fe_3Si) and two silicate phases: Mg_2SiO_4-ringwoodite (Si^{IV}) and $MgSiO_3$-perovskite (Si^{VI}). All calculations are based on lattice-dynamical estimates of the effects of silicon isotope substitution on vibrational (phonon) energies, sampling phonon densities of states at discrete phonon wave vectors and unit-cell volumes. Phonon Grüneisen parameters are used to construct a quasiharmonic equation of state for each phase, allowing a correction for thermal pressure. In agreement with previous modeling (Georg et al., 2007) our new results indicate that silicate will have higher $^{30}Si/^{28}Si$ than coexisting metal. At 10 GPa, ringwoodite–metal fractionation decreases from 1.4‰ at 2000 K to 0.6‰ at 3000 K (Fig. 5). Silicate melts are expected to have mainly Si^{IV} at $P \leq 10$ GPa (Stixrude and Karki, 2005), and likely exhibit a similar range of fractionations. Calculated forsterite–metal and diopside-metal fractionations appear to be 0.1–0.2‰ larger over this temperature range. Remarkably, the calculated perovskite-metal fractionation at 135 GPa is almost coincident with the low pressure trend. This suggests that the increase in silicon coordination in high pressure silicate melts – normally expected to decrease phonon frequencies and thus the silicate–metal fractionation factor – is largely compensated by increases in the phonon frequencies with pressure.

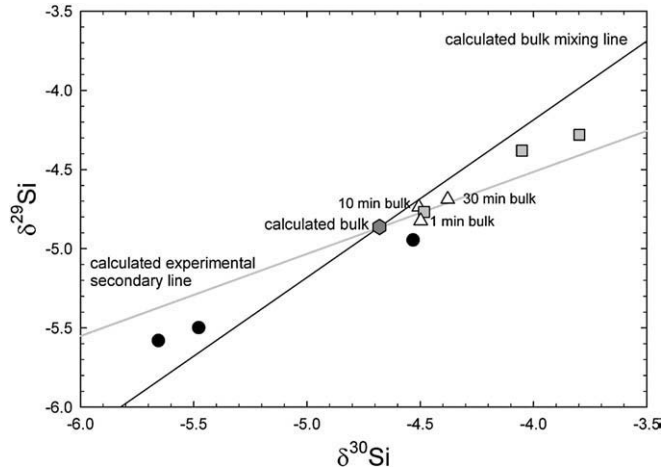

Fig. 4. The silicon isotopic data shown in Fig. 3, along with the bulk isotopic composition of each experiment. The bulk value for each experiment is different due to Si loss to the graphite capsules, explaining the drift in the data off the expected secondary fractionation line. Symbols: gray line: calculated secondary fractionation line; black line: calculated mixing line; triangles: bulk values; squares: silicate data points; circles: metal data points, hexagon is the calculated bulk value.

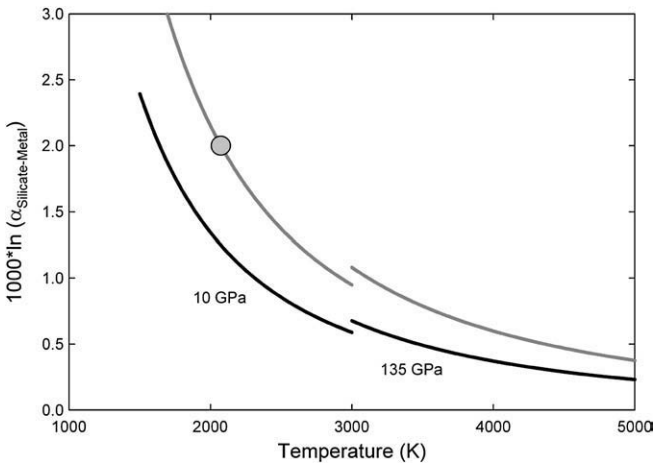

Fig. 5. Equilibrium silicate–metal $^{30}Si/^{28}Si$ fractionation at 10 GPa and 135 GPa. The black lines represent the theoretical curve while the gray lines are scaled theoretical curves, fit to our new experiments (shown by the gray circle). $\alpha_{Silicate-Metal} = (^{30}Si/^{28}Si)_{Silicate}/(^{30}Si/^{28}Si)_{Metal}$. The 10 GPa calculation is based on lattice-dynamics models for ringwoodite (γ-Mg_2SiO_4) and Fe_3Si. The 135 GPa calculation compares perovskite ($MgSiO_3$) and Fe_3Si.

Reconnaissance calculations on the 5-coordinate silicon site in α-$CaSi_2O_5$ (Kudoh and Kanzaki, 1998) indicate fractionation characteristics intermediate between those for Si^{IV} and Si^{VI}.

Our experiments provide an anchor to the calculations described above. At 1 GPa and 1800 °C the predicted fractionation between Si in silicate melt and Fe melt is 1.2‰ compared with our measured value of 2‰ (Fig. 5). We consider this to be a good agreement given the uncertainties in these types of calculations. The utility of the calculations, however, lies in their ability to examine the effects of pressure and temperature not yet accessed experimentally rather than providing accurate fractionation factors. If we use the theoretical calculations to extrapolate our experimental result to 2500 K and 25 GPa (possible core–mantle equilibration conditions) by fitting the A/T^2 curve through the experimental datum, and recognizing that the pressure effects are small, a fractionation of 1.2‰ results, leading to 6 wt% Si in the core (Eq. (3)). The exact fraction of Si in the core calculated using Eq. (3) depends on the exact difference between chondrite and bulk Earth $^{30}Si/^{28}Si$. This caveat notwithstanding, the $\Delta^{30}Si_{silicate-metal}$ we observe in our experiments gives considerable leverage on detecting Si in the core. For example, if the Fitoussi et al. (2009) measurements are correct rather than the Georg et al. (2007) measurements, then extrapolation of our experimental result combined with Eq. (3) gives 2 wt% Si in the core. If there is no measurable difference in $^{30}Si/^{28}Si$ between Earth and meteorites, then uncertainties correspond to a detection limit of 1.3 wt% Si. Our experiments combined with the extrapolations to core formation conditions require that there should be substantial Si isotope fractionation between Earth's metallic core and silicate rock if there is Si in the core.

5. Conclusions

We have produced the first experimental evidence for a silicon isotope fractionation between metal and silicate melt at high pressure and temperature by combining state-of-the-art techniques in isotope geochemistry and experimental petrology. The result provides an independent constraint on the silicon content in the core that is in the range of previous estimates based on geophysical and cosmochemical observations. Our results provide insight into silicon isotope fractionation during the core formation of the proto-Earth and multi-stage planetary formation processes through collisions of planetesimals and small planetary bodies. Further experiments at higher pressure will provide a quantitative foundation for using stable isotopes as monitors of planet formation processes.

Acknowledgements

The paper was improved following thoughtful reviews by Bastian Georg and Ben Reynolds and editorial work by Lars Stixrude. This work was supported by NSF Geochemistry grant to YF (EAR-0738741), NSF (EAR0711411) to EDY and NSF (EAR0643286, EAR0345433 and EAR0711411) to EAS.

References

Armytage, R.M.G., Georg, R.B., Halliday, A.N., 2009. The non-chondritic silicon isotope composition of the bulk silicate earth. Lunar and Planetary Science Conference XL, Abstract # 1167.

Badro, J., Fiquet, G., Guyot, F., Gregoryanz, E., Occelli, F., Antonangeli, D., d'Astuto, M., 2007. Effect of light elements on the sound velocities in solid iron: Implications for the composition of Earth's core. Earth Planet. Sci. Lett. 254, 233–238.

Bauer, O., Deiss, E., 1915. Translated from German by William T. Hall and Robert S. Williams, The Sampling and Chemical Analysis of Iron and Steel, (McGraw Hill Book Co. Inc., London).

Bigeleisen, J., Mayer, M.G., 1947. Equilibrium constants for isotopic exchange reactions. J. Chem. Phys. 15, 261–267.

Birch, F., 1964. Elasticity and constitution of the Earth's interior. J. Geophys. Res. 69, 4377–4388.

Birch, F., 1952. Density and composition of mantle and core. J. Geophys. Res. 57, 227–286.

De La Rocha, C.L., Brzezinski, M.A., DeNiro, M.J., 1996. Purification, recovery, and laser-driven fluorination of silicon dissolved and particulate silica for the measurement of natural stable isotope abundances. Anal. Chem. 68, 3746–3750.

Douthitt, C.B., 1982. The geochemistry of the stable isotopes of silicon. Geochim. Cosmochim. Acta 46, 1449–1458.

Dubrovinsky, L., Dubrovinskaia, N., Langenhorst, F., Dobson, D., Rubie, D., Gessman, C., Abrikesov, I.A., Johansson, B., Baykov, V.I., Vitos, L., Le Bihan, T., Grcichton, W.A., Dmitniev, V., Weber, H.-P., 2003. Iron–silica inter-action at extreme conditions and the electrically conducting layer at the base of Earth's mantle. Nature 422, 58–61.

Fitoussi, C., Bourdon, B., Kleine, T., Oberli, F., Reynolds, B. C., 2009. Si isotope systematics of meteorites and terrestrial peridotites: implications for Mg/Si fractionation in the solar nebula and for Si in the Earth's core. Earth Planet. Sci. Lett. 287, 77–85.

Georg, R.B., Halliday, A.N., Schauble, E.A., Reynolds, B.C., 2007. Silicon in the Earth's core. Nature 447, 1102–1106.

Georg, R.B., Reynolds, B.C., Frank, M., Halliday, A.N., 2006. New sample preparation techniques for the determination of Si isotopic composition using MC-ICPMS. Chem. Geol. 235, 95–104.

Ito, E., Morooka, K., Ujike, O., Katsura, T., 1995. Reactions between molten iron and silicate melts at high pressure: implications for the chemical evolution of Earth's core. J. Geophys. Res. 100, 5901–5910.

Knittle, E., Jeanloz, R., 1989. Simulating the core–mantle boundary: an experimental study of high-pressure reactions between silicates and liquid iron. Geophys. Res. Lett. 16, 609–612.

Kudoh, Y., Kanzaki, M., 1998. Crystal chemical characteristics of α-$CaSi_2O_5$, a new high pressure calcium silicate with five-coordinated silicon synthesized at 1500 ºC and 10 GPa. Phys. Chem. Miner. 25, 429–433.

Li, J., Fei, Y., 2004. Experimental Constraints on Core Composition. Treatise on Geochemistry, Volume 2, Chapter 14.

Lin, J.F., Heinz, D.L., Campbell, A.J., Devine, J.M., Shen, G.Y., 2002. Iron–silicon alloy in Earth's core? Science 295, 313–315.

Matsuhisa, Y., Goldsmith, J.R., Clayton, R.N., 1978. Mechanisms of hydrothermal crystallization of quartz at 250C and 15 kbar. Geochim. Cosmochim. Acta 42, 173–182.

O'Neil, H.S.C., 1991. The origin of the moon and the early history of the Earth — a chemical model. Part 1: the moon. Geochim. Cosmochim. Acta 55, 1135–1157.

Palme, H., O'Neil, H.S.C., 2003. Cosmochemical estimates of mantle composition. In: Holland, H.D., Turekian, K.K. (Eds.), Treatise on Geochmistry. Elsevier, Amsterdam. vol. 2, chap. 1.

Polyakov, V.I., 2009. Equilibrium iron isotope fractionation at core-mantle boundary conditions. Science 323, 912–914.

Polyakov, V.B., Kharlashina, N.N., 1994. Effect of pressure on equilibrium isotopic fractionation. Geochim. Cosmochim. Acta 58, 4739–4750.

Poitrasson, F., Roskosz, M., Corgne, A., 2009. No iron isotope fractionation between molten alloys and silicate melt to 2000C and 7.7 GPa: experimental evidence and implications for planetary differentiation and accretion. Earth Planet. Sci. Lett. 278, 376–385.

Reynolds, B.C., Aggarwal, J., André, L., Baxter, D., Beucher, C., Brzezinski, M.A., Engström, E., Georg, R.B., Land, M., Leng, M.J., Opfergelt, S., Rodushkin, I., Sloane, H.J., van den Boorn, S.H.J.M., Vroon, P.Z., Cardinal, D., 2007. An inter-laboratory comparison of Si isotope reference materials. J. Anal. At. Spectrom. 22, 561–568.

Ringwood, A.E., 1989. Significance of the terrestrial Mg/Si ratio. Earth Planet. Sci. Lett. 95, 1–7.

Shahar, A., Young, E.D., Manning, C.E., 2008. Equilibrium high-temperature Fe isotope fractionation between fayalite and magnetite: an experimental calibration. Earth Planet. Sci. Lett. 268, 330–338.

Stixrude, L., Karki, B., 2005. Structure and freezing of $MgSiO_3$ liquid in Earth's lower mantle. Science 310, 297–299.

Thibault, Y., Walter, M.J., 1995. The influence of pressure and temperature on the metal-silicate partition coefficients of nickel and cobalt in a model C1 chondrite and implications for metal segregation in a deep magma ocean. Geochim. Cosmochim. Acta 59, 991–1002.

Wänke, H., Dreibus, G., 1997. New evidence for silicon as the major light element in the Earth's core. Lunar and Planetary Science Conference XXVIII, p. 1280.

Zuckerman, B., Koester, D., Melis, C., Hansen, B.M., Jura, M., 2007. The chemical composition of an extrasolar minor planet. Astrophys. J. 671, 872–877.